J Mater Sci: Mater Med (2010) 21:3085–3093
DOI 10.1007/s10856-010-4170-x

A dynamic mechanical thermal analysis study of the viscoelastic properties and glass transition temperature behaviour of bioresorbable polymer matrix nanocomposites

Samuel I. J. Wilberforce · Serena M. Best · Ruth E. Cameron

Received: 1 May 2010 / Accepted: 18 October 2010 / Published online: 28 October 2010

Abstract The application of bioresorbable polymer nanocomposites in orthopaedics offer the potential to address several of the limitations associated with the use of metallic implants. Their enhanced biological performance has been demonstrated recently, but until now relatively little work has been reported on their mechanical properties. To this end, the viscoelastic properties and T_g of bioresorbable polylactide-co-glycolide/α-tricalcium phosphate nanocomposites were investigated by dynamic mechanical thermal analysis. At room temperature of approximately 20°C, the storage moduli of the nanocomposites were generally higher than the storage modulus of the unfilled polymer due to the stiffening effect of the nano-particles. However at physiological temperature of approximately 37°C, the storage moduli of the nanocomposites decreased from 6.2 to 15.4% v/v nano-particle loadings. Similarly the T_g of the nanocomposites also decreased from 6.2 to 15.4% v/v nano-particle loadings. These effects were thought to be due to weak interfacial bonding between the nano-particles and polymer matrix. The storage moduli at 37°C and T_g increased from the minimum value when the particle loading was raised to 25.7 and 34.2% v/v loadings. SEM and particle size distribution histograms showed that at these loadings, there was a broad particle size distribution consisting of nano-particles and micro-particles and that some particle agglomeration was present. The consequent reduction in the interfacial area and the number of weak interfaces presumably accounts for the rise in the storage modulus at 37°C and the T_g.

S. I. J. Wilberforce (✉) · S. M. Best · R. E. Cameron
Department of Materials Science and Metallurgy, Cambridge Centre for Medical Materials, University of Cambridge, New Museums Site, Pembroke Street, Cambridge CB2 3QZ, UK
e-mail: sijw2@cam.ac.uk

1 Introduction

A number of biodegradable and bioactive polymer matrix composites (PMCs) have been proposed as bone graft substitutes [1–3]. Recently, biological studies that have been carried out on these nanocomposites have revealed enhanced biological response and degradation [2, 4]. When implanted, these composites can give temporary support to the body allowing new bone tissue to form naturally. Bone is a biological nanocomposite [5]. Therefore, in order to closely mimic the exceptional qualities of bone, it may be desirable for these biodegradable PMCs to have nano-scale fillers. There are a number of important properties of polymer materials that can be used to determine the suitability of biodegradable polymer matrix nanocomposites (PMNCs) for load bearing applications, such as for bone graft substitutes. The dynamic viscoelastic properties, such as storage modulus (E′) and glass transition temperature (T_g) are some of these key properties of polymer materials that can be used to determine the suitability of biodegradable polymer matrix nanocomposites (PMNCs) for load bearing applications.

Conflicting results have been reported concerning the dependence of dynamic mechanical properties and T_g of PMNCs on nano-particle loading. The E′, T_g, damping factor (tan δ) and activation energy (E_a) for glassy relaxation of various PMNCs were found to increase with increasing nano-particle loading [6–8]. This was attributed to the hindrance of the motion of the polymer chain segments by the nano-particles. However it has been reported that the T_g and E′ of other PMNCs decreased with

increasing nano-particle loading [6, 9–14]. The T_g depression was attributed to the creation of a large interfacial zone with increasing nano-filler loading, leading to dispersed regions of high chain mobility [11]. It was postulated that these regions served to break up the percolation pathways of slower dynamical regions, which led to a large reduction in T_g [11].

Since the fracture of bone occurs under dynamic loading, the dynamic viscoelastic properties of bone may have a prominent effect during the fracture process [15]. It is therefore useful to investigate the dynamic viscoelastic behaviour of biodegradable PMNCs which have the potential to be used for bone graft substitutes. The viscoelastic properties and T_g of bioresorbable PMNCs investigated by dynamic mechanical thermal analysis (DMTA) have been reported [6, 8]. However there are no reported results on the dynamic viscoelastic properties and T_g of polylactide-co-glycolide/α-tricalcium phosphate (PLGA/α-TCP) nanocomposites. Therefore the DMTA technique was used in this study to investigate the dynamic viscoelastic properties and T_g behaviour of a family of bioresorbable PLGA/α-TCP nanocomposites intended for use as bone graft substitutes in which the level of particle addition was varied. This work forms part of a large study, which has characterized in detail the biological and degradation behaviours of these nanocomposites [2, 4]. This present study now focuses on the important consideration of the effects of nanocomposite formulations on dynamic mechanical properties.

2 Materials and methods

2.1 Materials

A 50:50 M ratio bioresorbable PLGA was purchased from Lakeshore Biomaterials, Alabama, USA. The PLGA had a molecular weight of 65 kDa and an inherent viscosity of 0.47 dl/g. The α-TCP filler in powder form was prepared in-house via an aqueous precipitation reaction followed by high temperature calcining process. Acetone of analytical reagent grade (obtained from BDH Laboratory Supplies, UK) was used as the solvent in the preparation of the PLGA/α-TCP nanocomposites.

2.2 Preparation of α-TCP filler

TCP was prepared by an aqueous precipitation reaction between 98% $Ca(OH)_2$ and 85% ortho-H_3PO_4 at a molar ratio of 3:2 [3]. The dried TCP cake was ground and calcined at 1400°C to obtain the α-TCP phase using the following calcining program: heating at 2.5°C/min to 1400°C, dwelling for 4 h at 1400°C and cooling at a rate of 20°C/min to 20°C.

2.3 Preparation of PLGA/α-TCP nanocomposites

A modified solvent evaporation (MSE) method [2, 16] via attrition milling (continuously working agitator attritor shaft bead mill (model PE 075/PR 01) from Netzsch-Feinmahltechnik GmbH, Germany) was employed to break up and disperse varying weight fractions of nano-α-TCP powder in 50:50 M ratio bioresorbable PLGA prior to piston injection moulding. Acetone was used as the solvent in the MSE process. Attrition milling of nano α-TCP powder was carried out for 2 h in acetone with 2 mm diameter spherical alumina beads. This was followed by gradual dissolving of PLGA in the nano α-TCP/acetone solution with milling for a further 30 min. Attritor milling of unfilled PLGA only in acetone for 30 min was also carried out. The attritor-milled materials were dried in air in Teflon containers for 2–4 days to evaporate the acetone. This was followed by further drying in a vacuum oven at a temperature of 50°C and a vacuum pressure of 800 mbar for approximately 4 days to remove any residual acetone.

Dumbbell-shaped specimens of as received PLGA, attritor-milled PLGA and nanocomposites were produced with a piston type 12 cubic centimetre (12 cc) mini injection moulding machine from DSM Xplore, Geleen, The Netherlands using the following processing conditions: barrel temperature = 140°C, mould temperature = 35°C, holding pressure = 8 bars, injection pressure = 6 bars and holding time = 3 s. The injection moulded (IM) specimens had nominal dimensions of length = 74 mm, width = 5 mm and thickness = 2 mm. The IM dumbbell-shaped specimens were machined into uniform rectangular bars for DMTA. The IM attritor-milled (att-mill) unfilled PLGA was used as the control sample.

2.4 SEM of IM PLGA materials

Cold cathode field emission electron gun type SEM (cFEG-SEM) (S-5500 from Hitachi, Japan) at an accelerating voltage of 2 kV was used to characterize the morphology of the IM nanocomposites and the dispersion state of the α-TCP nano-particles in the PLGA matrix. The specimens for SEM were obtained by freezing the samples in liquid nitrogen. Samples for SEM were then chipped off from gauge length region of the dumbbell shaped specimens in liquid nitrogen using a sharp razor blade and hammer. The nanocomposite specimens were viewed in low angle back-scattered electrons (LA-BSE—LA100) mode. This allowed the α-TCP particles (seen as whitish pattern on the SEM micrograph) to be differentiated from the PLGA matrix (seen as greyish background on the SEM micrograph). The

LA-BSE micrographs were obtained from at least four different regions of each nanocomposite sample. At least 20 LA-BSE micrographs were obtained for the nanocomposites and at least 100 particle sizes in total were measured from the micrographs using the image processing and analysis in Java (ImageJ 1.42q/Java 1.6.0_10 [32-bit]) software to determine the particle size distribution of the α-TCP particles in PLGA.

Using the particle size distribution histograms of the IM nanocomposites, the surface area of the α-TCP nano-particles in the PLGA matrix was calculated with the following equations with the assumption that the particles are spheres:

$$v_p = \frac{\sum_{d=d_{\min}}^{d=d_{\max}} n_d\left(\frac{4}{3}\pi r_d^3\right)}{\sum_{d=d_{\min}}^{d=d_{\max}} n_d} \quad (1)$$

where v_p = average volume of one particle, n_d = number of particles obtained from the frequency of each particle and r_d = radius of each particle obtained from the diameter of the particle = d/2. Using v_p, the number of particles per unit volume of nanocomposite (N) was calculated with the following equation:

$$N = \frac{\%v/v}{v_p} \quad (2)$$

where % v/v is the volume fraction of α-TCP nano-particles in the PLGA matrix. The surface area of one particle (S_p) was also calculated with the following equation:

$$S_p = \frac{\sum_{d=d_{\min}}^{d=d_{\max}} n_d\left(4\pi r_d^2\right)}{\sum_{d=d_{\min}}^{d=d_{\max}} n_d} \quad (3)$$

The surface area of all particles per unit volume composite (S) was calculated using the following equation:

$$S = N \times S_p \quad (4)$$

A plot of S^{-1} versus % v/v was obtained to illustrate the relationship between the surface area of the nano-particles in the PLGA matrix and % v/v of nano-particles.

2.5 TGA of IM PLGA materials

Thermogravimetric analysis (TGA) (model TGA Q500 from TA Instruments, Delaware, USA) was employed to measure the actual weight fraction of α-TCP filler particles in the IM specimens and to verify the absence or presence of residual acetone in the IM materials. The thermal decomposition temperatures (TDT) of the IM PLGA materials were also obtained from TGA. Nitrogen and air were used as the balance gas and sample gas respectively for the TGA experiments. A pre-weighed amount of material between 5 and 15 mg was heated at a rate of 10°C/min from about 12 to 600°C. The IM nanocomposites were assigned the following names according to the nominal weight fraction of α-TCP particles in PLGA: IM PLGA10, IM PLGA20, IM PLGA30, IM PLGA40 and IM PLGA50. The actual weight fractions, w_f (% w/w), as determined from TGA were subsequently converted into volume fractions, Φ_f (% v/v), using Eq. 5.

$$\Phi_f = \left[1 + \frac{\rho_f}{\rho_m}\left(\frac{1}{w_f} - 1\right)\right]^{-1} \quad (5)$$

where ρ_m is the density of 50:50 PLGA (= 1.33 g cm^{-3} [17]) and ρ_f is the measured density of nano-α-TCP (= 2.81 g cm^{-3} [18]).

2.6 DMTA of IM PLGA/α-TCP nanocomposites

DMTA (DMA Q800 from TA Instruments, Delaware, USA) was carried out on the IM specimens to investigate their dynamic viscoelastic properties and T_g. DMTA tests were carried out in cantilever mode using a dual cantilever clamp at oscillation amplitude of 15 μm. A multi-frequency-strain module was employed at varying frequencies of 1, 5, 10, 20, 50 and 100 Hz. The temperature was swept at a heating rate of 3°C/min from −25 to 100°C and the measurements made at intervals of 2°C. During the measurements, the sample was held isothermally for 5 min.

3 Results

3.1 TGA

The TGA thermograms of the IM PLGA materials are reported in Fig. 1. The % w/w and % v/v of α-TCP particles in the PLGA matrix are also reported in Table 1. The TGA thermograms of the IM PLGA materials showed a one stage decomposition profile and also confirmed the absence of residual acetone in the IM att-mill unfilled PLGA and IM nanocomposites. The actual % w/w of the α-TCP nano-particles in the PLGA matrix as determined from the TGA thermogram for each nanocomposite were reasonably close to their nominal % w/w values. The TDT (Table 1) of the IM PLGA materials was determined from their TGA thermograms at the temperature corresponding to 80% w/w weight loss.

3.2 Dispersion state, morphology and particle size distribution

The LA-BSE micrographs and the histograms showing the morphology and dispersion state as well as particle size distribution respectively of the α-TCP particles in the

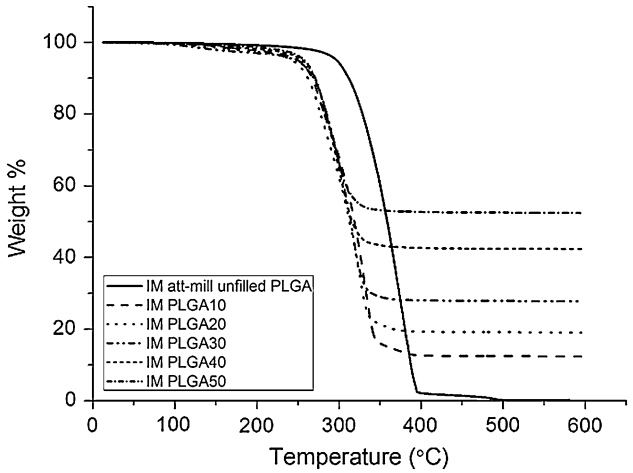

Fig. 1 TGA thermograms of the IM PLGA materials showing one stage decomposition profile and the absence of residual acetone in the IM att-mill unfilled PLGA and IM nanocomposites

Table 1 % w/w and % v/v of α-TCP in PLGA and TDT at 80% w/w of the IM PLGA materials

Sample	% w/w of α-TCP	% v/v of α-TCP	TDT (80% w/w)
IM att-mill unfilled PLGA	0.0	0.0	328.6
IM PLGA10	12.4	6.2	282.2
IM PLGA20	19.0	10.0	277.7
IM PLGA30	27.8	15.4	285.3
IM PLGA40	42.3	25.7	284.3
IM PLGA50	52.4	34.2	284.7

PLGA matrix for each IM nanocomposite are reported in Figs. 2, 3, 4, 5 and 6. The LA-BSE micrographs are typical of at least 20 images taken from at least 4 different regions of the IM nanocomposite samples.

3.3 DMTA

The E′ curves at 1 Hz for each IM material are reported in Fig. 7. Similar trends were observed at the other frequencies. The E′ values of the IM materials at room temperature of approximately 20°C and physiological temperature of approximately 37°C at a range of frequencies are reported in Fig. 8a, b respectively. The E′ values at the specified temperatures were calculated from the E′ curves by linear interpolation between two temperature points within which they lie. The peak temperature of the DMTA tan δ (= E″/E′) curve was taken as the T_g of the IM PLGA materials. The T_g at a range of frequencies for the IM materials are reported in Fig. 8c. The plot of S^{-1} versus % v/v is also reported in Fig. 8d.

4 Discussion

4.1 TDT, dispersion state, morphology and particle size distribution

The TGA thermograms (Fig. 1) of the IM PLGA materials showed that the thermogram of the IM att-mill unfilled PLGA shifted to a higher temperature than those of the IM PLGA nanocomposites. The TDT of the IM PLGA materials, which was taken as the temperature corresponding to 80% w/w on the thermogram, confirmed that the TDT of the IM PLGA nanocomposites were lower than the TDT of the IM att-mill unfilled PLGA. Other researchers have also reported lower TDT of polymer matrix nanocomposites than the TDT of the pure polymer phase [19–21], although the reason for this behaviour is not well understood.

The LA-BSE micrograph of IM PLGA10 (Fig. 2a) showed good dispersion of α-TCP particles in the PLGA matrix with slight agglomeration. The particle size distribution histogram of IM PLGA10 (Fig. 2b) showed that the α-TCP nano-particles had majority of the sizes well below 1000 nm. The highest frequency particle size was approximately 75 nm. The LA-BSE micrographs of IM PLGA20 and IM PLGA30 (Figs. 3a, 4a respectively) also confirmed good dispersion of the α-TCP nano-particles in the PLGA matrix albeit with more agglomerated particles than IM PLGA10. The particle size distribution histograms of IM PLGA20 and IM PLGA30 (Fig. 3b, 4b respectively) showed that the α-TCP nano-particles had majority of sizes below 1000 nm.

The highest frequency particle sizes for IM PLGA20 and IM PLGA30 were approximately 100 and 150 nm respectively. The LA-BSE micrographs of IM PLGA40 and IM PLGA50 (Figs. 5a, 6a respectively) showed a mix of α-TCP nano-particles and micro-particles with some agglomerated particles. The particle size distribution histograms of IM PLGA40 and IM PLGA50 (Figs. 5b, 6b respectively) confirmed a broad distribution of α-TCP particle sizes consisting of particle sizes below 1000 nm (nano-particles) and above 1000 nm (micro-particles). The highest frequency particle sizes for IM PLGA40 nd IM PLGA50 were approximately 225 and 325 nm respectively.

4.2 E′ and T_g

The E′ curves (Fig. 7) showed typical glassy, leathery and rubbery regions. At room temperature of approximately 20°C within the glassy region, the E′ of the nanocomposites were generally higher than the E′ of the IM att-mill unfilled PLGA (Fig. 8a) due to the stiffening effect of the α-TCP particles. However at physiological temperature of approximately 37°C, the E′ of the nanocomposites

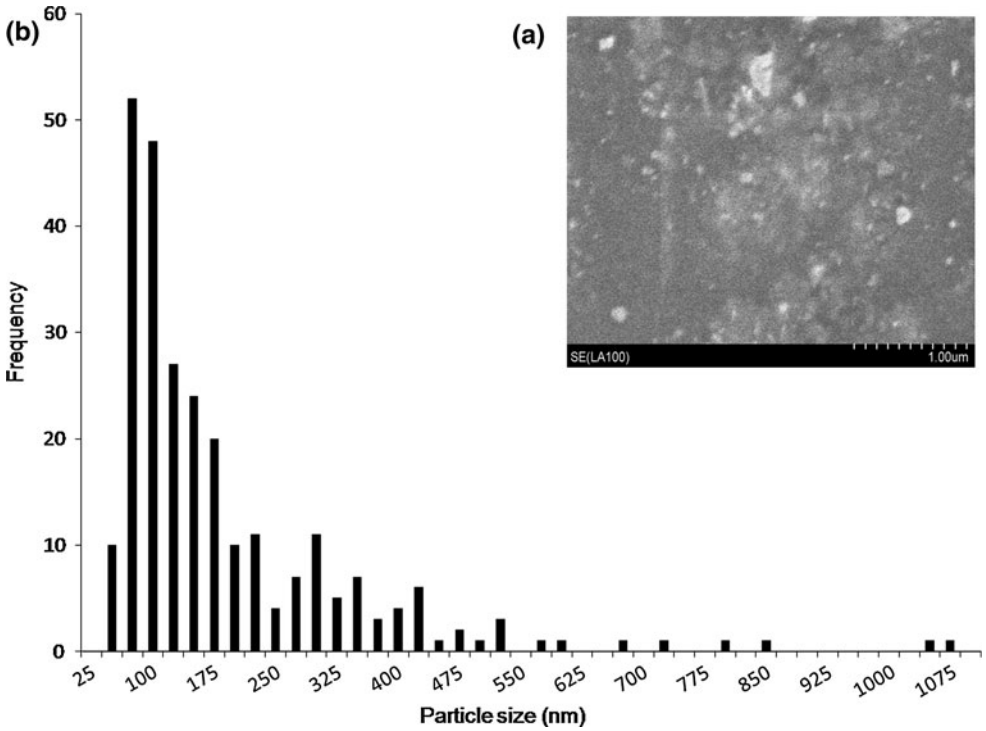

Fig. 2 **a** LA-BSE micrograph of IM PLGA10 and **b** histogram showing particle size distribution of α-TCP in IM PLGA10

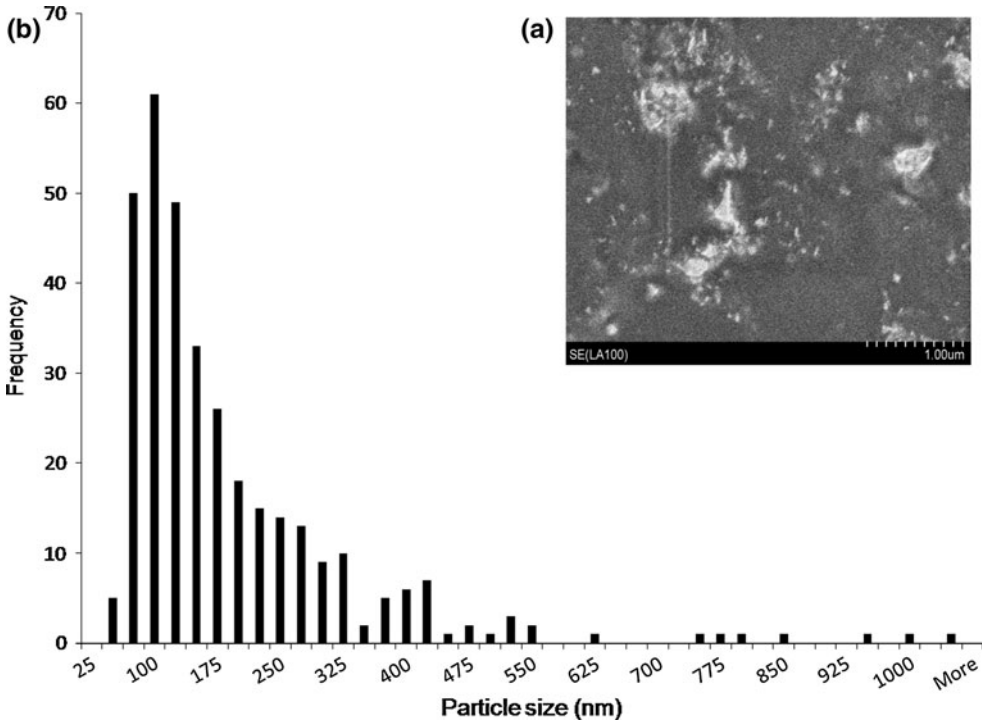

Fig. 3 **a** LA-BSE micrograph of IM PLGA20 and **b** histogram showing particle size distribution of α-TCP in IM PLGA20

decreased from the nanocomposite with α-TCP nano-particle loading of 6.2% v/v to nanocomposite with α-TCP nano-particle loading of 15.4% v/v (Fig. 8b). Likewise the T_g of the nanocomposites also decreased from 6.2 to 15.4% v/v α-TCP nano-particle loadings (Fig. 8c).

In order to explain the drop in these properties, the surface area per unit volume of nanocomposite (S) of the α-TCP nano-particles in the PLGA matrix was calculated using Eqs. 1–4, assuming that all the α-TCP nano-particles are spheres. It was thought that if an effect is interface

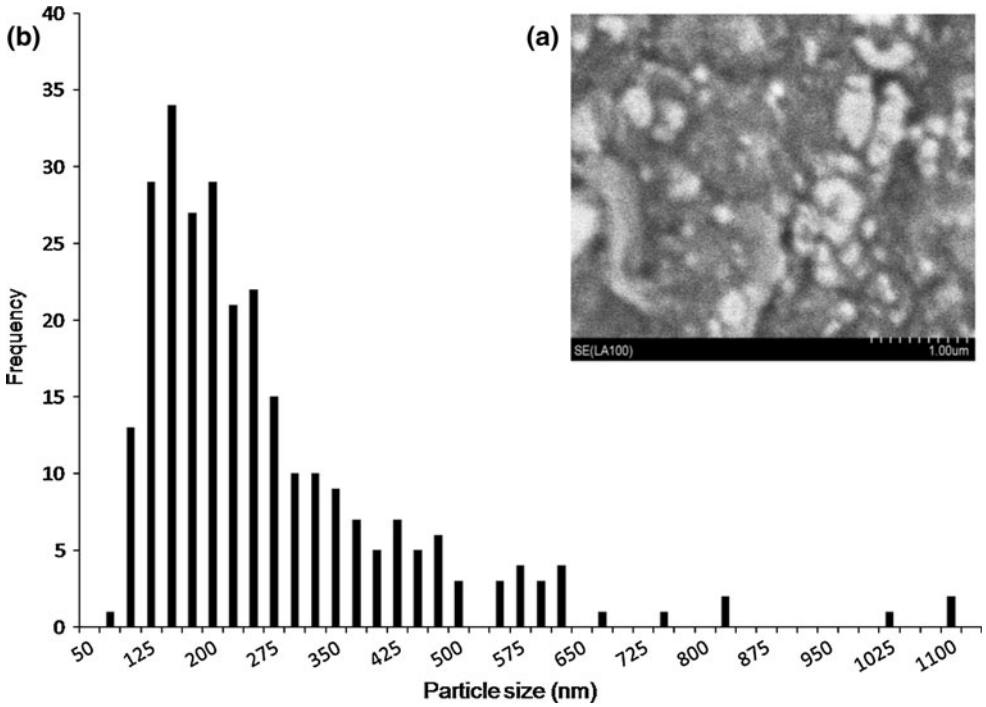

Fig. 4 **a** LA-BSE micrograph of IM PLGA30 and **b** histogram showing particle size distribution of α-TCP in IM PLGA30

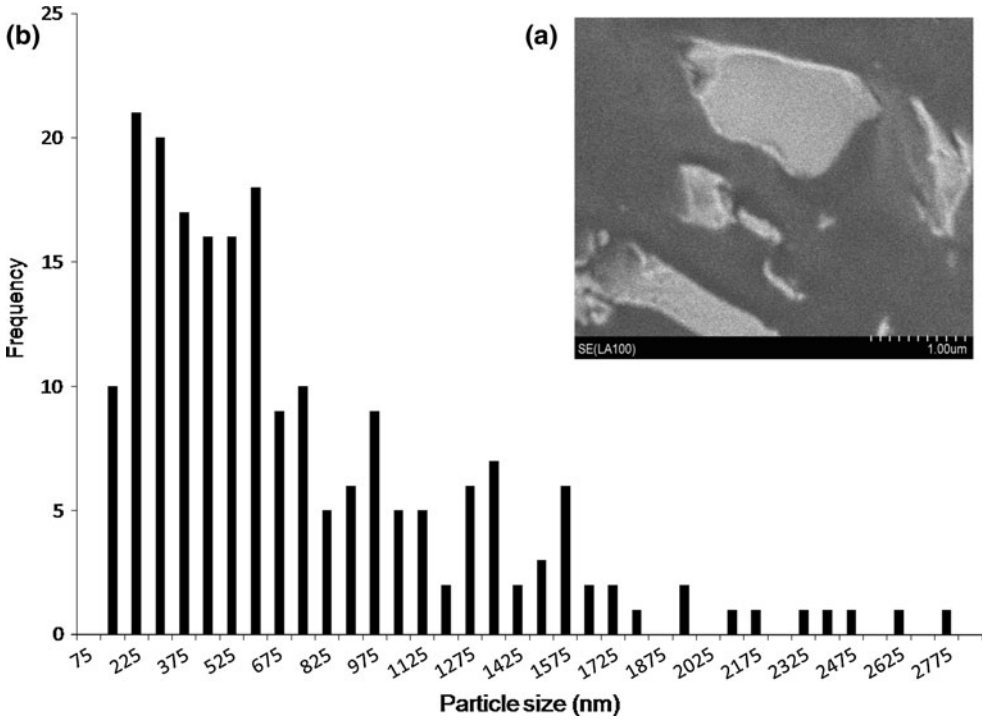

Fig. 5 **a** LA-BSE micrograph of IM PLGA40 and **b** histogram showing a broad particle size distribution of α-TCP in IM PLGA40

related (for example T_g), then it should be related to S. The value of S^{-1} of the α-TCP nano-particles decreased (corresponding to increasing S) with increasing % v/v up to 15.4% v/v (Fig. 8d). This is consistent with the theory that the T_g drop up to 15.4% v/v was due to an increase in PLGA/α-TCP nano-particle interface area, providing a large energetically unfavoured weak interfacial area due to the poor attraction between the polymer segments and nano-particles [11, 22]. The drop in the E′ at 37°C is likely to be related to this fall in T_g. Other authors have attributed similar decreases in the E′ to the presence of nano-particle agglomerates acting as defects or stress concentrators [6].

The E′ at 37°C and the T_g increased at 25.7 and 34.2% v/v loadings (Fig. 8b, c). The LA-BSE micrographs and

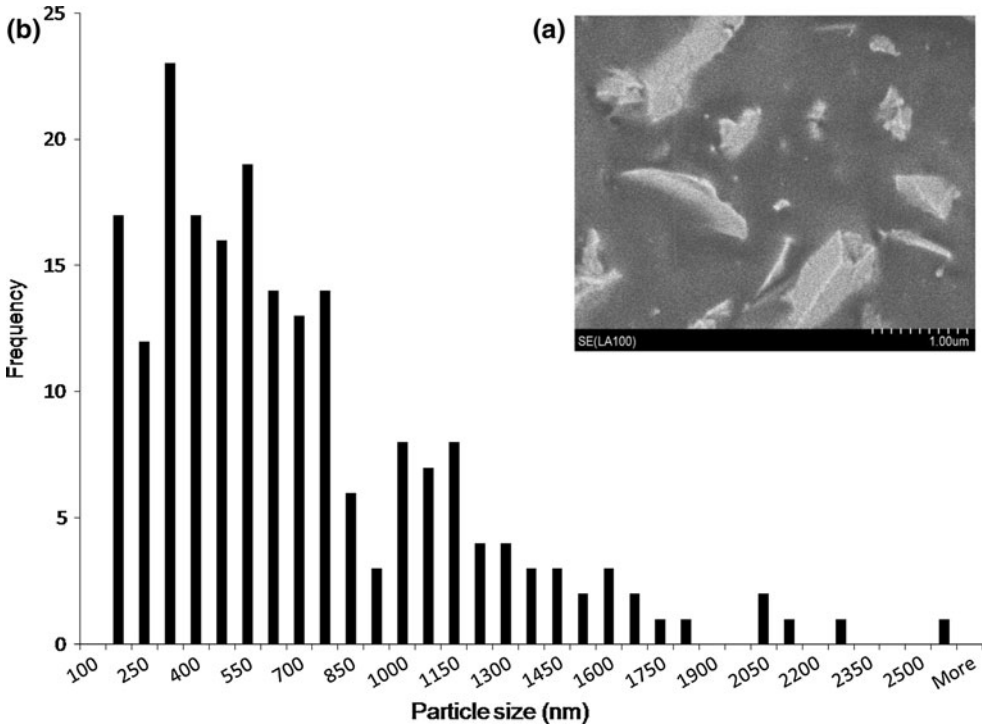

Fig. 6 **a** LA-BSE micrograph of IM PLGA50 and **b** histogram showing a broad particle size distribution of α-TCP in IM PLGA50

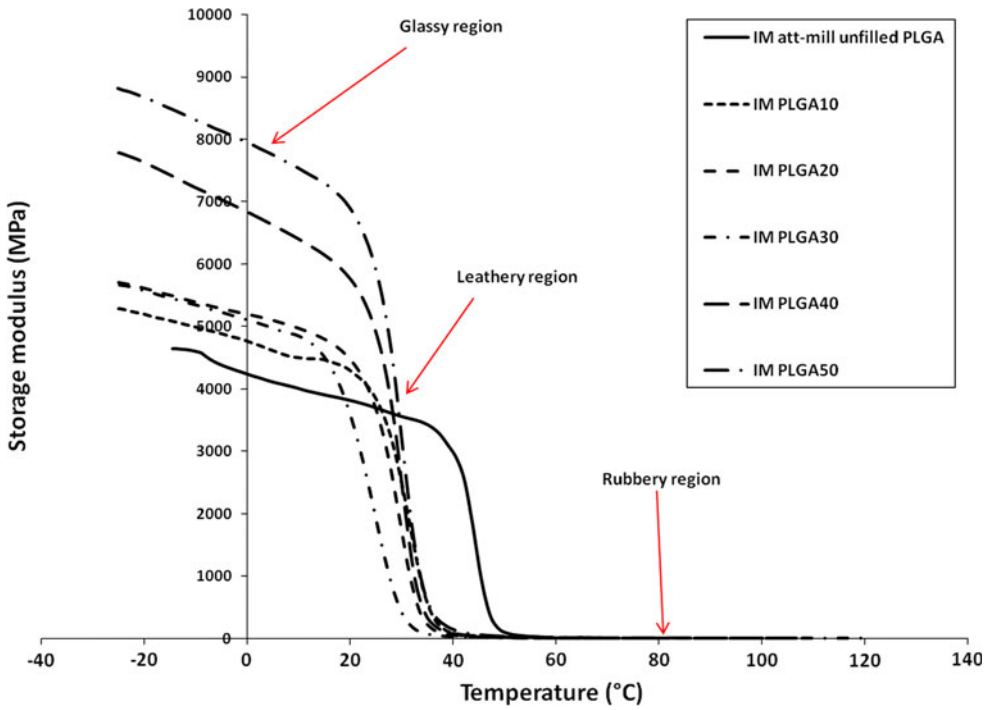

Fig. 7 E′ curves of IM PLGA materials at a frequency of 1 Hz showing three viscoelastic regions

particle size distribution histograms (Figs. 5, 6) of these materials confirmed that there was a broad α-TCP particle size distribution consisting of nano-particles and micro-particles and that some particle agglomeration was present. S^{-1} of the α-TCP particles in the PLGA matrix also increased at these loadings (corresponding to a decrease in S) (Fig. 8d). The consequent reduction in the interfacial area and the number of weak interfaces presumably accounts for the rise in the T_g at these loading levels. The rise in T_g also resulted in the increase in E′ at 37°C. Other researchers have attributed similar increases in E′ to jamming of nano-particle clusters or agglomerates and micro-particles at higher loadings [22–24].

At the tested frequencies, the E′ values of the nano-composites at physiological temperature of 37°C were found to be within the E′ range at 1 Hz for cancellous bone

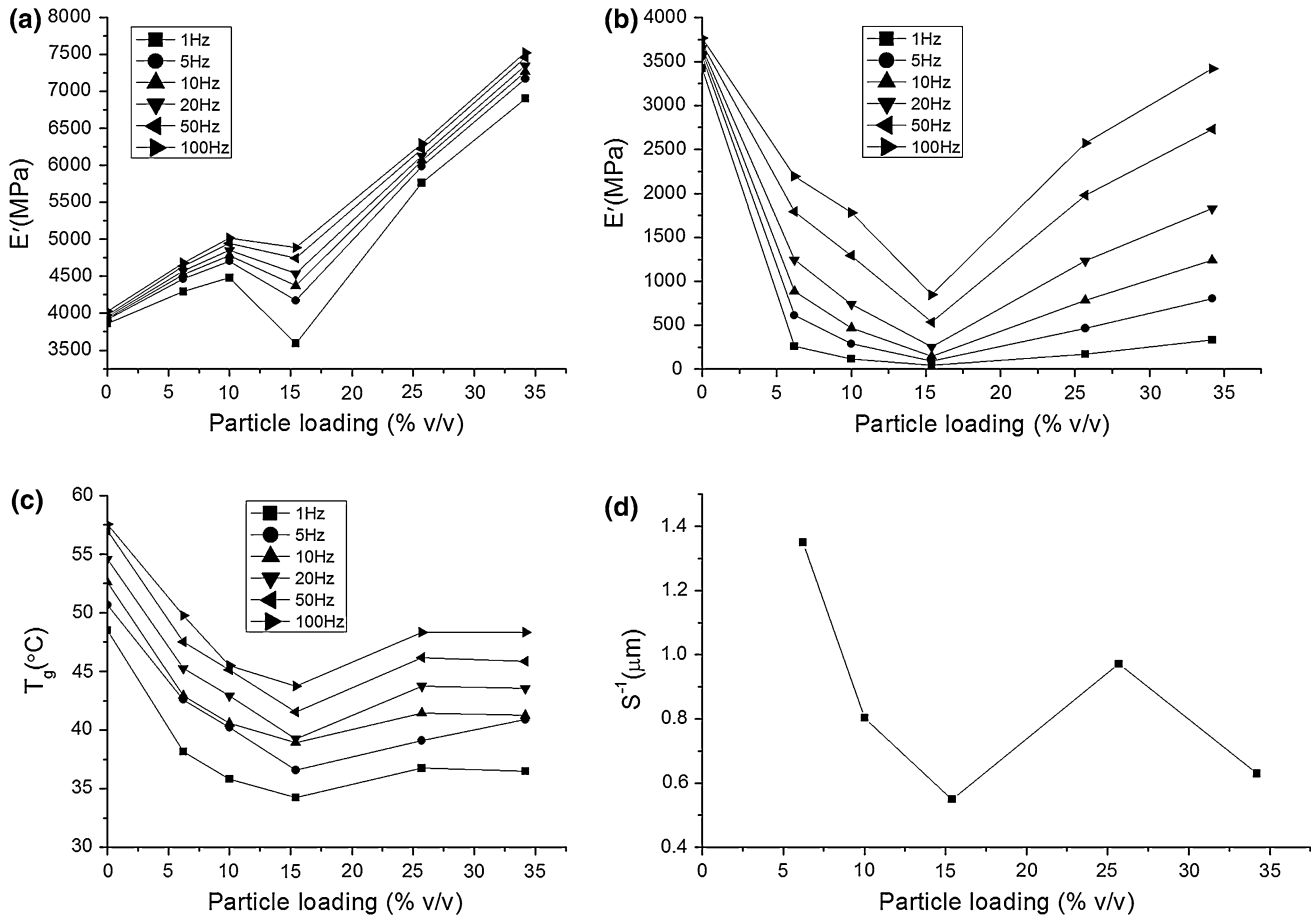

Fig. 8 **a** E′ values of IM att-mill unfilled PLGA and nanocomposites at 20°C, **b** E′ values of IM att-mill unfilled PLGA and nanocomposites at 37°C, **c** T_g of IM att-mill unfilled PLGA and nanocomposites at a range of frequencies and **d** S^{-1} versus % v/v of α-TCP nano-particles in PLGA

(50.0–500 MPa) [6, 25]. In fact at higher frequencies, the E′ values of the nanocomposites at 37°C were found to be higher than the higher end of the E′ range for cancellous bone, implying that if deformation occurs at higher frequencies during in vivo applications the nanocomposites will be able to generate enough energy to resist deformation due to the highly viscoelastic nature of the PLGA matrix. It should also be noted that the E′ values at 37°C were obtained at dry conditions and should be taken as indicative properties of the nanocomposites at near physiological conditions. A decrease in E′ is expected during in vivo usage due to wet conditions in the body.

Another important advantage of the E′ values being within the range for cancellous bone is that, stress shielding may be prevented during bone regeneration. Even though the T_g of the nanocomposites seemed to drop and gets close to 37°C, in particular at frequency of 1 Hz, this might be advantageous as it has been reported that tissue engineering materials with a T_g close to physiological temperature are recommended since materials with T_g higher than physiological temperature tend to be brittle and can fracture during in vivo use when subjected to stress [6, 26]. It seems then that at higher frequencies brittle fracture of the nanocomposites might occur during in vivo use since the T_g of the nanocomposites at higher frequencies are higher than the physiological temperature, however it is expected that the T_g will decrease close to physiological temperature in the presence of wet conditions during in vivo use.

5 Conclusion

At room temperature of approximately 20°C, the E′ of the nanocomposites were generally higher than that of the unfilled polymer control due to the stiffening effect of the α-TCP particles. However the E′ at 37°C and T_g of nanocomposites decreased from 6.2 to 15.4% v/v loadings before rising again at higher loadings of 25.7 and 34.2% v/v. This was thought to be due to a combination of the following effects: (1) weak interfacial bonding between the nano-particles and polymer matrix, which lowers T_g, and (2) the presence of micro-particles and agglomerated nano-particles at higher loading levels which reduces the effective surface area and number of weak interfaces, leading to

an increase in the E′ at 37°C and T_g. The E′ values at 37°C of the nanocomposites were within the E′ range for cancellous bone, however these are indicative values at near physiological conditions. It is expected that the E′ will drop during in vivo usage due to the presence of wet conditions in the body. It may be possible to reduce the lowering of the E′ at 37°C and T_g of the nanocomposites by surface modification of the α-TCP nano-particles to enhance the interfacial bonding or attraction with the polymer matrix segments.

Acknowledgements Samuel I. J. Wilberforce is grateful to his partner, Ms. Charlotte Fay von Karsa, for funding his PhD studies. The authors thank DSM Xplore for the use of their mini injection moulding machine. The authors also thank Prof. William Clegg of Cambridge University's Materials Science and Metallurgy department for the use of his attritor milling machine. Samuel I. J. Wilberforce is grateful for the support of Dr. Jenny Shepherd, Mr. David Shepherd, Mr. Rob Cornell and Mr. Simon Griggs also of Cambridge University's Materials Science and Metallurgy department during experiments. The authors are also grateful for the support of Mr. Jon Rickard of the Cavendish Laboratory, Department of Physics, University of Cambridge for his support during the SEM experiments.

References

1. Rezwan K, Chen QZ, Blaker JJ, Boccaccini AR. Biodegradable and bioactive porous polymer/inorganic composite scaffolds for bone tissue engineering. Biomaterials. 2006;27:3413–31.
2. Yang ZJ, Best SM, Cameron RE. The Influence of alpha-tricalcium phosphate nanoparticles and microparticles on the degradation of poly(D,L-lactide-co-glycolide). Adv Mater. 2009;21:3900–4.
3. Ehrenfried LM, Patel MH, Cameron RE. The effect of tri-calcium phosphate (TCP) addition on the degradation of polylactide-co-glycolide (PLGA). J Mater Sci Mater Med. 2008;19:459–66.
4. Yang Z, Thian ES, Brooks RA, Rushton N, Best SM, Cameron RE. Apatite formation on alpha-tricalcium phosphate/poly (D,L-lactide-co-glycolide) nanocomposite. Bioceramics. 2008;361–363:459–62.
5. Ji BH, Gao HJ. Mechanical properties of nanostructure of biological materials. J Mech Phys Solids. 2004;52:1963–90.
6. Jose MV, Thomas V, Johnson KT, Dean DR, Nyalro E. Aligned PLGA/HA nanofibrous nanocomposite scaffolds for bone tissue engineering. Acta Biomater. 2009;5:305–15.
7. Wu TM, Liu CY. Poly(ethylene 2, 6-naphthalate)/layered silicate nanocomposites: fabrication, crystallization behavior and properties. Polymer. 2005;46:5621–9.
8. Chen DZ, Tang CY, Chan KC, Tsui CP, Yu PHF, Leung MCP, et al. Dynamic mechanical properties and in vitro bioactivity of PHBHV/HA nanocomposite. Compos Sci Technol. 2007;67:1617–26.
9. Ash BJ, Siegel RW, Schadler LS. Mechanical behavior of alumina/poly(methyl methacrylate) nanocomposites. Macromolecules. 2004;37:1358–69.
10. Khan AN, Hong PD, Chuang WT, Shih KS. Effect of uniaxial drawing on the structure and glass transition behavior of poly(trimethylene 2,6-naphthalate)/layered clay nanocomposites. Polymer. 2009;50:6287–96.
11. Ash BJ, Siegel RW, Schadler LS. Glass-transition temperature behavior of alumina/PMMA nanocomposites. J Polym Sci B Polym Phys. 2004;42:4371–83.
12. Liu FK, Hsieh SY, Ko FH, Chu TC. Synthesis of gold/poly (methyl methacrylate) hybrid nanocomposites. Colloids Surf A Physicochem Eng Asp. 2003;231:31–8.
13. Ash BJ, Schadler LS, Siegel RW. Glass transition behavior of alumina/polymethylmethacrylate nanocomposites. Mater Lett. 2002;55:83–7.
14. Arrighi V, McEwen IJ, Qian H, Prieto MBS. The glass transition and interfacial layer in styrene-butadiene rubber containing silica nanofiller. Polymer. 2003;44:6259–66.
15. Wang T, Feng Z. Dynamic mechanical properties of cortical bone: The effect of mineral content. Mater Lett. 2005;59:2277–80.
16. Yang Z, Thian ES, Best SM, Cameron RE. A novel way of dispersing fine ceramic particles in PLGA matrix. Bioceramics. 2007;330–332:511–4.
17. Van de Velde K, Kiekens P. Biopolymers: overview of several properties and consequences on their applications. Polym Test. 2002;21:433–42.
18. Mathew M, Schroeder LW, Dickens B, Brown WE. Crystal-structure of alpha-Ca3(PO4)2. Acta Crystallogr B Struct Sci. 1977;33:1325–33.
19. Wu DF, Wu LA, Wu LF, Zhang M. Rheology and thermal stability of polylactide/clay nanocomposites. Polym Degrad Stab. 2006;91:3149–55.
20. Ogata N, Jimenez G, Kawai H, Ogihara T. Structure and thermal/mechanical properties of poly(l-lactide)-clay blend. J Polym Sci B Polym Phys. 1997;35:389–96.
21. Chang JH, An YU, Sur GS. Poly(lactic acid) nanocomposites with various organoclays. I. Thermomechanical properties, morphology, and gas permeability. J Polym Sci B Polym Phys. 2003;41:94–103.
22. Sen S, Thomin JD, Kumar SK, Keblinski P. Molecular underpinnings of the mechanical reinforcement in polymer nanocomposites. Macromolecules. 2007;40:4059–67.
23. Zhu ZY, Thompson T, Wang SQ, von Meerwall ED, Halasa A. Investigating linear and nonlinear viscoelastic behavior using model silica-particle-filled polybutadiene. Macromolecules. 2005;38:
8816–24.
24. Pryamitsyn V, Ganesan V. Origins of linear viscoelastic behavior of polymer-nanoparticle composites. Macromolecules. 2006;39:844–56.
25. Murugan R, Ramakrishna S. Development of nanocomposites for bone grafting. Compos Sci Technol. 2005;65:2385–406.
26. Park PIP, Jonnalagadda S. Predictors of glass transition in the biodegradable polylactide and poly-lactide-co-glycolide polymers. J Appl Polym Sci. 2006;100:1983–7.